

Analysis of the anomalous doppler effect from quantum theory to classical dynamics simulations

Xinhang Xu(徐新航)¹, Jinlin Xie(谢锦林)^{1,†}, Jian Liu(刘健)², and Wandong Liu(刘万东)¹

¹Department of Plasma Physics and Fusion Engineering, University of Science and Technology of China, Hefei 230026, China

²Weihai Institute for Interdisciplinary Research, Shandong University, Weihai 264209, China

(Received 12 May 2025; revised manuscript received 13 June 2025; accepted manuscript online 27 June 2025)

The fundamental physics of anomalous and normal Doppler resonances between electrons and electromagnetic (EM) waves is analyzed using a quantum model that incorporates angular-momentum conservation. This work extends prior theory by explicitly linking the resonant integer m to the EM wave's angular-momentum quantum number. Numerical simulations based on the volume-preserving algorithm (VPA) further confirm this correspondence. Moreover, a direct comparison of the energy-transfer ratio from translational energy to gyrokinetic energy during resonance, between classical dynamics and quantum predictions, is presented and verified numerically.

Keywords: anomalous Doppler effect, resonant condition, angular momentum conservation

PACS: 03.65.-w, 33.35.+r, 02.60.Cb, 12.20.-m

DOI: [10.1088/1674-1056/ade8e4](https://doi.org/10.1088/1674-1056/ade8e4)

CSTR: [32038.14.CPB.ade8e4](https://cstr.iopscience.iop.org/32038.14.CPB.ade8e4)

1. Introduction

The anomalous Doppler effect (ADE),^[1–5] in which the observed frequency shift behaves contrary to the conventional Doppler effect under specific conditions, was first theoretically predicted by Soviet physicist Ginzburg.^[4] This phenomenon arises when a system moves with a velocity exceeding the phase velocity of light in the medium, transferring its translational kinetic energy into internal energy while emitting radiation. A notable example, discussed by Frank in his 1958 Nobel lecture,^[2] shows that radiation emission does not occur through the typical transition from an excited state to a lower energy level. Instead, it proceeds from a lower to a higher energy level, powered by the system's translational kinetic energy. This counterintuitive prediction has attracted considerable attention and has inspired extensive research.^[6–14]

In 1967, Artsimovich *et al.*^[15] reported discrepancies in tokamak experiments: the electron temperature estimated from diamagnetic signals was significantly higher than that derived from electrical-conductivity measurements. Although unrecognized at the time, this anomaly may represent the first experimental observation of ADE. In 1968, Kadomtsev and Pogutse^[16] identified ADE as the underlying mechanism, in which electrons undergo velocity scattering from the longitudinal to the transverse direction under resonant conditions. This process enhances the diamagnetic effect beyond what would be expected from thermal motion alone. Subsequently, a range of ADE-related phenomena have been observed, including electron-beam scattering in magnetic-field vacuum tubes,^[2] wave radiation,^[17–19] and runaway-electron instabilities in tokamaks.^[20,21] The ADE has also given rise to prac-

tical applications, notably in high-power microwave generation and in mitigating runaway electrons in tokamak fusion reactors.^[11,22]

The physics of the ADE was first elucidated through quantum analysis by Frank^[2] and Ginzburg.^[23] In this work, we extend Ginzburg's quantum framework by incorporating the conservation of angular momentum to provide a more rigorous analysis of ADE. This approach yields new insights into the relationship between wave angular momentum and ADE under resonant conditions, which is referred to as anomalous Doppler resonance (ADR). For an electron moving in a magnetic field and interacting with an external electromagnetic (EM) wave, the general resonance condition is given by

$$\omega = m\omega_{ce} + \mathbf{k} \cdot \mathbf{v},$$

where \mathbf{k} is the wave vector, ω_{ce} is the electron cyclotron frequency (here $\omega_{ce} > 0$), \mathbf{v} is the electron velocity, and ω is the wave angular frequency, while $m = 0, \pm 1, \pm 2, \pm 3, \dots$ represents the Landau level.^[26] Specifically, for plane EM waves, we find that resonance is restricted to the fundamental harmonics ($m = \pm 1$) due to spin angular-momentum conservation, reducing the condition to

$$\omega = \pm \omega_{ce} + \mathbf{k} \cdot \mathbf{v},$$

where the negative sign refers to the ADR condition, while the positive sign refers to the normal Doppler resonance (NDR) condition. This represents a significant constraint compared to previous theoretical treatments^[41] which suggested possible resonance at all harmonic orders ($m = \pm 1, \pm 2, \dots$) for plane

[†]Corresponding author. E-mail: jlxie@ustc.edu.cn

EM wave. Despite the simplicity of the model, our analysis demonstrates that angular-momentum conservation plays a crucial role in EM wave-electron resonance — an aspect that, to the best of our knowledge, has not been previously addressed in the literature.

Furthermore, we perform numerical simulations of a single electron interacting resonantly with an EM wave in the presence of uniform static electric and magnetic fields, using classical equations of motion. These simulations elucidate the relationship between wave angular momentum and the resonance mechanism. Additionally, we compute the energy-transfer ratio from the electron's translational kinetic energy to its gyrokinetic energy during resonance, and the results show strong agreement with predictions from quantum theory.

The remainder of this paper is organized as follows. Section 2 develops the quantum theoretical framework incorporating angular-momentum conservation. Section 3 presents our numerical approach, detailing the simulation setup, analyzing the time evolution of electron velocity and kinetic energy, investigating the resonant conditions with wave angular momentum, and examining the energy-transfer ratio and polarization characteristics. Section 4 provides a comprehensive discussion of the key findings and their physical implications. Finally, Section 5 summarizes the principal conclusions and outlines potential directions for future research.

2. Quantum analysis of ADE

When a charged particle moves through a medium at a speed greater than the phase velocity of light in that medium, it induces polarization in the surrounding molecules. As these molecules return to their equilibrium state, they emit electromagnetic radiation. The constructive interference of these emissions produces the characteristic Cherenkov radiation, forming a cone-shaped wavefront, as shown in Fig. 1. The direction of Cherenkov radiation is constrained to the Cherenkov radiation angle $\theta_0 = \arccos\left(\frac{c'}{v}\right)$, where c' is the speed of light in the medium and v is the velocity of the charged particle.

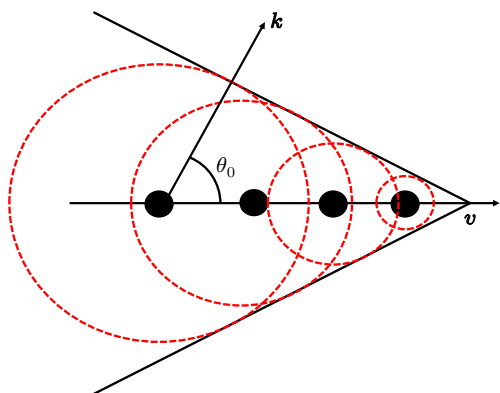


Fig. 1. Schematic diagram of Cherenkov radiation. The black points indicate snapshots of the electron at different times, the red dashed circle represents the current radiation surface from the previous electron.

However, when the electron is replaced by a system possessing internal energy — such as an oscillator or a cyclotron electron in a magnetic field — the direction of the emitted photon is no longer determined by the interference of secondary waves and can instead occur in any direction. Considering a scenario in which the system emits a photon with angular frequency ω and wavevector k , the emission process must satisfy both energy and momentum conservation:

$$T_1 + U_1 = \hbar\omega + T_2 + U_2, \quad (1a)$$

$$\mathbf{p}_1 = \mathbf{p}_2 + \hbar\mathbf{k}. \quad (1b)$$

Here, T and U represent the kinetic energy and internal energy of the system, while the subscripts 1 and 2 refer to the states before and after emitting a photon. \mathbf{p} denotes the momentum of the system, and \hbar represents the reduced Planck constant. Assuming that the photon's energy is far less than the initial kinetic energy T_1 , the loss of kinetic energy after photon emission can be written as $\Delta T_{12} = T_1 - T_2 = \Delta\mathbf{p} \cdot \mathbf{v}$, where \mathbf{v} is the velocity of the system before emission and $\Delta\mathbf{p} = \mathbf{p}_1 - \mathbf{p}_2 = \hbar\mathbf{k}$. Thus, the change in internal energy becomes

$$\Delta U_{21} = \Delta T_{12} - \hbar\omega = \hbar\mathbf{k} \cdot \mathbf{v} - \hbar\omega = \hbar\omega \left(\frac{v \cos \theta}{c'} - 1 \right). \quad (2)$$

Here, $\omega/k = c'$, and $\Delta U_{21} = U_2 - U_1$. When the system's velocity exceeds the speed of light in the medium ($v > c'$), the sign of ΔU_{21} allows the radiation to be categorized into three distinct regions, as illustrated in Fig. 2.

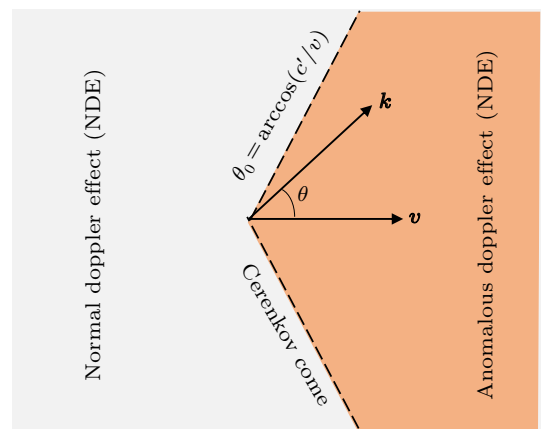


Fig. 2. Regions of the ADE and the NDE .

(i) For $\theta > \theta_0 = \arccos(c'/v)$, $\Delta U_{21} < 0$. The system produces photons by consuming both its internal and kinetic energy; this region corresponds to the normal Doppler effect (NDE).

(ii) For $\theta = \theta_0$, $\Delta U_{21} = 0$, and the loss of kinetic energy by the system is completely converted into photon energy; this line corresponds to the Cherenkov Effect.

(iii) For $\theta < \theta_0$, $\Delta U_{21} > 0$. This region is referred to as the ADE, where the system gains internal energy after emitting photons. This means that the loss of kinetic energy is converted into both photon energy and internal energy.

In previous work, the change in internal energy was given as $\Delta U = m\hbar\omega_{ce}$, where $m = 0, \pm 1, \pm 2, \pm 3, \dots$ represents the Landau level, as reported by Ginzburg,^[25] Coppi,^[26] Frolov,^[27] Frank,^[2] Tamm^[1] and Nezlin.^[6] The above discussion revisits the foundational work of Ginzburg.^[25] In the present paper, it is further demonstrated that m actually corresponds to the quantum number associated with the angular momentum of the emitted photon.

Let us consider the process in which an electron cyclotron system under a uniform magnetic field emits a photon along the z axis, as shown in Fig. 3. The moving electron has velocity v_z along the background magnetic field and cyclotron velocity v_{\perp} . The kinetic energy along z is $T = \gamma m_0 c^2 - m_0 c^2$, where γ denotes the Lorentz factor and m_0 refers to the electron's rest mass. The internal energy is approximated expressed as $U = \frac{1}{2} \gamma m_0 v_{\perp}^2$.

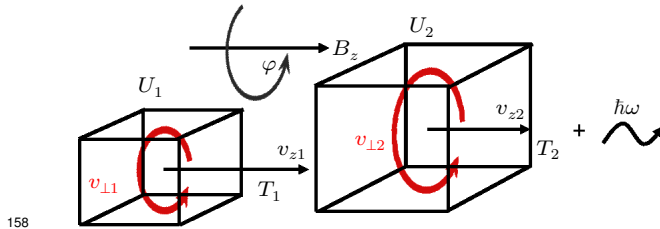


Fig. 3. Schematic diagram of the electron cyclotron system before and after photon emission. Here, $U_2 > U_1$ and $T_2 < T_1$.

Assume the angular momentum of the system before and after emitting a photon is L_1 and L_2 , respectively. The angular momentum of the photon is $m\hbar$. According to angular-momentum conservation, we have

$$L_1 = L_2 + m\hbar. \quad (3)$$

Since the magnetic field is aligned along the z direction, the angular momentum of the electron along z is represented as L_z . According to quantum theory, the electron wave in a static magnetic field can be expressed as

$$\Psi = \Psi_0 e^{i(\mathbf{p}-e\mathbf{A}) \cdot \mathbf{s}}, \quad (4)$$

where Ψ_0 is the normalization coefficient, \mathbf{A} is the vector potential, and \mathbf{s} is the position. For a gyrating electron in a magnetic field, $\mathbf{s} = r\phi \mathbf{e}_\phi$, where r is the cyclotron radius and ϕ is the cyclotron angle.

The z -component of the orbital angular momentum operator can be expressed in spherical coordinates as

$$\hat{L}_z = -i\hbar \frac{\partial}{\partial \phi}. \quad (5)$$

Combining Eq. (4) with Eq. (5), we have

$$-i\hbar \frac{\partial}{\partial \phi} \Psi = (p_\phi - eA_\phi) r \Psi. \quad (6)$$

As a result, the eigenvalue of L_z can be expressed as

$$L_z = (p_\phi - eA_\phi)r. \quad (7)$$

With $p_\phi = \gamma m_0 v_{\perp}$, $A_\phi = \frac{rB_0}{2}$, and $r = \frac{\gamma m_0 v_{\perp}}{B_0 e}$, Eq. (7) can be rewritten as

$$L_z = \frac{1}{2} \cdot \frac{\gamma m_0 v_{\perp}^2}{\omega_{ce}} = \frac{U}{\omega_{ce}}, \quad (8)$$

where $\omega_{ce} = \frac{eB}{m_0 \gamma} = \frac{\omega_0}{\gamma}$ and $U = \frac{1}{2} \gamma m_0 v_{\perp}^2$. Here, m_0 is the electron rest mass, γ is the Lorentz factor, and ω_0 is the electron cyclotron frequency in the rest frame (here we choose $\omega_0 > 0$). The conservation of angular momentum in the z -direction is expressed as

$$L_{z2} + m\hbar = L_{z1}.$$

The variation in the angular momentum of the electron along the z -axis is given by

$$\Delta L_{21} = L_{z2} - L_{z1} = \frac{U_2 - U_1}{\omega_{ce}} = -m\hbar. \quad (9)$$

Here, m is the quantum number of the photon's angular momentum in the z -direction. The internal-energy change is given by $\Delta U_{21} = U_2 - U_1$. With Eq. (9), it can be rewritten as

$$\Delta U_{21} = -m\hbar\omega_{ce}. \quad (10)$$

According to Eqs. (2) and (10), the change in electron energy can be written as

$$\hbar\mathbf{k} \cdot \mathbf{v} = \hbar\omega - m\hbar\omega_{ce}. \quad (11)$$

This result is consistent with previous findings.^[1,2,6,24,26,27] Here, $\hbar\mathbf{k} \cdot \mathbf{v}$ represents the loss of kinetic energy ΔT_{12} , $\hbar\omega$ represents the photon energy, and $-m\hbar\omega_{ce}$ represents the change in electron gyrokinetic energy ΔU_{21} . The ratio between the internal-energy change ΔU_{21} and the kinetic-energy change ΔT_{21} is

$$\frac{\Delta U_{21}}{\Delta T_{21}} = \frac{m\hbar\omega_{ce}}{\hbar\mathbf{k} \cdot \mathbf{v}}. \quad (12)$$

This result is a critical criterion for comparison with the classical dynamic simulation in Section 2. It is also derived from classical theory in the Appendix. After simplifying Eq. (11), we finally obtain the classical wave-particle resonance condition

$$\omega = k_z v_z + m\omega_{ce}. \quad (13)$$

The variable m represents the quantum number associated with the angular momentum of the photon. Since a photon possesses both orbital angular momentum ($l\hbar$, where $l =$

216 $0, \pm 1, \pm 2, \pm 3, \dots$) and intrinsic spin angular momentum ($s\hbar$,
 217 where $s = \pm 1$),^[28] the total angular momentum can be ex-
 218 pressed as $m\hbar = l\hbar + s\hbar$.

219 For photons carrying only spin angular momentum, two
 220 distinct quantum states are possible, characterized by the spin
 221 quantum number m :

222 (i) For $m = +1$ ($\Delta U_{21} < 0$), the cyclotron electron loses
 223 internal energy upon photon emission. The emitted photon ex-
 224 hibits right-hand circular polarization. This process is known
 225 as the NDE.

226 (ii) For $m = -1$ ($\Delta U_{21} > 0$), the cyclotron electron gains
 227 internal energy through photon emission. The emitted pho-
 228 ton exhibits left-hand circular polarization (the difference be-
 229 tween our definition of circular polarization and the standard
 230 definition^[3] stems from our choice of $\omega_0 > 0$). Here, $m > 0$
 231 corresponds to the same rotational sense as the electron's natu-
 232 ral right-hand gyration, yielding right-hand polarization when
 233 $\mathbf{k} \parallel \mathbf{B}_0$). This process corresponds to the ADE.

234 The above discussion describes spontaneous emission
 235 phenomena of ADE and NDE without external-field interven-
 236 tion. In our simulation model, we introduce an external plane
 237 EM wave that serves as a resonant field interacting with elec-
 238 trons. This plane EM wave acts as an inducing field, enabling
 239 a gyro-electron to undergo stimulated absorption or emission
 240 processes. From a quantum perspective, the plane EM wave
 241 can be regarded as an ocean of photons that carry only spin
 242 angular momentum. Consequently, the same resonance condi-
 243 tions as those derived from quantum field theory are recovered:

244 (i) Right-hand circularly polarized waves correspond to
 245 $m = +1$ states,^[39] resonating only when $\omega = \omega_{ce} + \mathbf{k} \cdot \mathbf{v}$ (NDE
 246 condition).

247 (ii) Left-hand circularly polarized waves correspond to
 248 $m = -1$ states, resonating only when $\omega = -\omega_{ce} + \mathbf{k} \cdot \mathbf{v}$ (ADE
 249 condition).

250 This exact correspondence between our classical simula-
 251 tion framework and quantum field-theoretic predictions vali-
 252 dates our modeling approach while providing physical insight
 253 into the angular-momentum selection rules governing these
 254 resonant interactions.

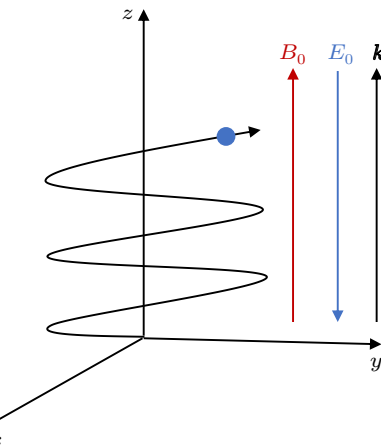
255 Although nonlinear analyses of electron interactions with
 256 electromagnetic waves have been extensively studied,^[29–37]
 257 the specific role of static electric fields in these interactions
 258 has received comparatively less attention. In our approach,
 259 the uniform electric field serves a crucial function by system-
 260 atically scanning the electron velocity, thereby enabling inves-
 261 tigation across the full spectrum of resonance conditions. The
 262 inherent complexity of these nonlinear processes precludes an-
 263 alytical solutions, necessitating the use of numerical simula-
 264 tion methods to obtain meaningful physical insights.

265 3. Classical dynamic simulation of ADR

266 The ADE process has been theoretically analyzed in the
 267 quantum framework, where the angular momentum carried by
 268 the emitted photon determines the resonance condition. To
 269 validate these characteristics in a classical picture, we investi-
 270 gate the interaction between an electromagnetic wave and an
 271 electron during ADR and NDR. The corresponding energy-
 272 transfer ratio can also be examined through numerical simula-
 273 tions.

274 3.1. Numerical simulation setup

275 To analyze the resonant process from the perspective of
 276 classical dynamics and to facilitate a direct comparison with
 277 the quantum results, we consider the following configuration.
 278 A uniform magnetic field \mathbf{B}_0 is applied along the z -direction.
 279 An electrostatic field \mathbf{E}_0 , oriented opposite to \mathbf{B}_0 (as illus-
 280 trated in Fig. 4), is introduced to accelerate the electron.



281 **Fig. 4.** Schematic of the setup: a uniform static magnetic field B_0 along
 282 the z -axis, an electrostatic field E_0 oriented opposite to B_0 , and a wavevector \mathbf{k} aligned parallel to B_0 .

283 We consider the interaction between an electron enter-
 284 ing the system with velocity v_z , parallel to the magnetic field
 285 $B_0 = B_z$, and a linearly or circularly polarized transverse elec-
 286 tromagnetic (TEM) wave propagating in a homogeneous di-
 287 electric medium with a refractive index $n > 1$.

288 The induced linearly polarized wave along \mathbf{B}_0 can be de-
 289 composed into a combination of a right-hand circularly polar-
 290 ized wave ($m = 1$) and a left-hand circularly polarized wave
 291 ($m = -1$), such that $\mathbf{E}_w = \mathbf{E}_R + \mathbf{E}_L$, where $\mathbf{E}_R = \frac{1}{2}\mathbf{E}_0(e_x +$
 292 $i\mathbf{e}_y)\exp[i(\mathbf{k} \cdot \mathbf{r} - \omega t)]$, $\mathbf{E}_L = \frac{1}{2}\mathbf{E}_0(e_x - i\mathbf{e}_y)\exp[i(\mathbf{k} \cdot \mathbf{r} - \omega t)]$.
 293 The magnetic field of the EM wave is

$$294 \quad \mathbf{B}_w = \frac{\mathbf{k} \times \mathbf{E}_w}{\omega}. \quad (14)$$

295 The six-dimensional phase space of an electron, de-
 296 scribed by its position \mathbf{r} and momentum \mathbf{p} , is governed by
 297 the equations below. The vectors \mathbf{E} and \mathbf{B} represent the total
 298 field, including both static and electromagnetic components.

299 Here, c denotes the speed of light in vacuum, e represents the
 300 electron's charge, and m_0 is the electron's rest mass

$$301 \quad \frac{dr}{dt} = \frac{\mathbf{p}}{\sqrt{m_0^2 + \frac{\mathbf{p}^2}{c^2}}},$$

$$302 \quad \frac{dp}{dt} = -e \left(\mathbf{E}(\mathbf{r}, t) + \frac{\mathbf{p}}{\sqrt{m_0^2 + \frac{\mathbf{p}^2}{c^2}}} \times \mathbf{B}(\mathbf{r}, t) \right). \quad (15)$$

303 To simulate the evolution of \mathbf{r} and \mathbf{p} , the above system is
 304 discretized using the Volume-Preserving Algorithm.^[9,38] Let
 305 j denote the iteration step and $\text{Cay}(\mathbf{A})$ represent the Cayley
 306 transform of matrix \mathbf{A}

$$307 \quad \begin{cases} \mathbf{r}_{j+\frac{1}{2}}^* = \mathbf{r}_j^* + \frac{\Delta t^*}{2\gamma_j} \mathbf{p}_j^*, \\ \mathbf{p}^{*-} = \mathbf{p}_j^* + \frac{\Delta t^*}{2} \mathbf{E}_{j+\frac{1}{2}}^*, \\ \mathbf{p}^{*+} = \text{Cay} \left(\frac{\Delta t^* \hat{\mathbf{B}}^*}{2\gamma^{*-}} \right) \mathbf{p}^{*-}, \\ \mathbf{p}_{j+1}^* = \mathbf{p}^{*+} + \frac{\Delta t^*}{2} \mathbf{E}_{j+\frac{1}{2}}^*, \\ \mathbf{r}_{j+1}^* = \mathbf{r}_{j+\frac{1}{2}}^* + \frac{\Delta t^*}{2\gamma_{j+1}} \mathbf{p}_{j+1}^*. \end{cases} \quad (16)$$

308 The dimensionless parameters are momentum $p^* = p/(m_0 c)$,
 309 magnetic field $B^* = B/(e\tau_{ce} m_0)$, total electric field $E^* =$
 310 $E/[m_0 c/(\tau_{ce} e)]$, time step $\Delta t^* = \Delta t/\tau_{ce}$, and position $r^* =$
 311 $r/(\tau_{ce} c)$, where τ_{ce} is the electron cyclotron period ($\tau_{ce} =$
 312 $2\pi/\omega_{ce}$) and $\gamma^* = \sqrt{1 + p^{*2}}$ is the Lorentz factor. The dimen-
 313 sionless magnetic matrix $\hat{\mathbf{B}}^*$ ^[38] is written as

$$314 \quad \hat{\mathbf{B}}^* = \begin{pmatrix} 0 & B_z^* & -B_y^* \\ -B_z^* & 0 & B_x^* \\ B_y^* & -B_x^* & 0 \end{pmatrix}. \quad (17)$$

315 To illustrate the system evolution, the parameters are set as
 316 follows: background magnetic field $B_0 = 0.02$ T, wave an-
 317 gular frequency $\omega_s = 1.5\omega_0$ where $\omega_0 = eB_0/m_0$, wavevec-
 318 tor $\mathbf{k} = 10^5$ m⁻¹, electric field component of the electro-
 319 magnetic wave $E_w = 9$ V/m. The induced wave propagates
 320 along the z axis with linear polarization, and the electrostatic
 321 field is $E_0 = -2.5$ V. The time step is chosen to satisfy
 322 $\Delta t = \min \left(\frac{2\pi}{50(\mathbf{k} \cdot \mathbf{v})}, \frac{2\pi}{50\omega_0}, \frac{2\pi}{50\omega_s} \right)$ to ensure simulation accuracy.

323 The evolution of the electron's motion is shown in Fig. 5.
 324 As the electron accelerates from rest in the electrostatic field
 325 (Fig. 5(b)), the resonant frequencies increase simultaneously
 326 (Fig. 5(a)). The change in parallel velocity caused by the
 327 electromagnetic wave can be quantified as $\Delta v = v_z - v_{zE_0}$
 328 (Fig. 5(c)), where v_z represents the parallel velocity under the
 329 combined fields, while v_{zE_0} denotes the parallel velocity result-
 330 ing solely from the electrostatic field, which can be calculated
 331 as

$$332 \quad v_{zE_0} = \frac{eE_0 t}{m_0 \sqrt{1 + \left(\frac{eE_0 t}{m_0 c} \right)^2}}. \quad (18)$$

333 The cyclotron velocity is shown in Fig. 5(d). The work
 334 done by the electromagnetic wave is shown in Fig. 5(e),
 335 which can be calculated by integrating the power over time
 336 as $E_{||\text{emw}} = \int P_{||\text{emw}} dt$, where $P_{||\text{emw}} = -e(\mathbf{v}_\perp \times \mathbf{B}_{\perp\text{emw}}) \cdot \mathbf{v}_z$.
 337 Since all discrete data points are available from the simulation,
 338 numerical integration is straightforward. Figure 5(f) shows the
 339 gyrokinetic energy evolution over time, where $E_\perp = \frac{1}{2} m_0 v_\perp^2$.

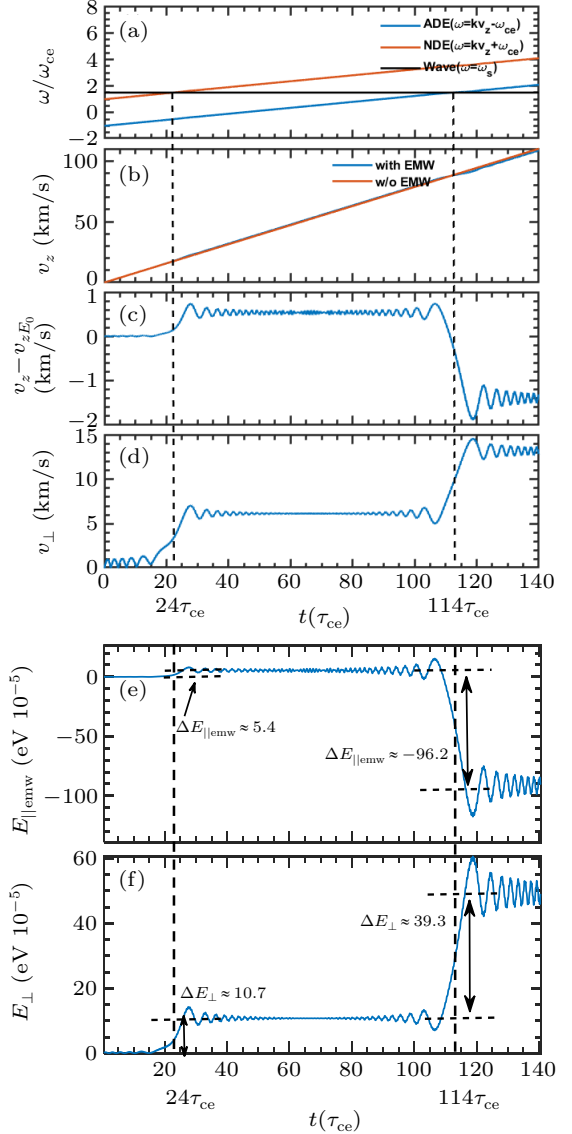


Fig. 5. Kinetic evolution of electrons in a magnetic field under the influence of an electromagnetic wave during acceleration. (a) Frequencies of ADE, NDE, and the source wave. (b) Parallel velocity v_z with and without the electromagnetic wave. (c) Change in parallel velocity induced by the electromagnetic wave. (d) Cyclotron velocity v_\perp . (e) Parallel kinetic energy transferred to the electron by the electromagnetic wave. (f) Evolution of gyrokinetic (perpendicular) energy.

342 3.2. Validation of energy transfer ratio

343 As shown in Fig. 5(a), around $23\tau_{ce}$, the normal Doppler
 344 frequency matches that of the induced wave, resulting in a
 345 rapid increase in the cyclotron velocity v_\perp (Fig. 5(b)). Si-
 346 multaneously, the change in parallel velocity induced by the
 347 electromagnetic wave also increases. This behavior can be in-
 348 terpreted as the electron cyclotron system absorbing a photon

349 during the NDR, leading to an increase in both parallel kinetic
350 energy and gyro-kinetic energy (internal energy).
399 (LHCP) wave ($m = -1$) induces a velocity change only around
400 $113\tau_{ce}$. This confirms that the RHCP wave corresponds to the
401 NDE, while the LHCP wave corresponds to the ADE, in agree-
402 ment with the quantum analysis.

351 The change in parallel kinetic energy due to the electro-
352 magnetic wave is shown in Fig. 5(e), where $\Delta T_{21} = \Delta E_{||\text{emw}} \approx$
353 5.4×10^{-5} eV. The corresponding increase in gyro-kinetic
354 energy is $\Delta U_{21} = \Delta E_{\perp} \approx 10.7 \times 10^{-5}$ eV, also shown in
355 Fig. 5(e). Consequently, the energy transfer ratio between
356 internal energy and parallel kinetic energy during resonance
357 is $\frac{\Delta U_{21}}{\Delta T_{21}} \approx 1.98$. According to quantum theory (Eq. (12)), for
358 $m = 1$ (NDE) and $k = 10^5 \text{ m}^{-1}$ along the z -axis, the resonant
359 velocity is $v_z \approx 19 \times 10^3 \text{ m/s}$ and $\omega_{ce} \approx 3.51 \times 10^9 \text{ s}^{-1}$. This
360 yields $n_p = 1.85$, in close agreement with the simulation re-
361 sults.
362

363 The ADR begins to manifest at $t \approx 113\tau_{ce}$, where $\omega_{ADE} =$
364 ω (Fig. 5(a)). At this point, the parallel velocity starts to scat-
365 ter into the perpendicular direction, as evidenced by the de-
366 crease in Δv_z and the corresponding increase in v_{\perp} (Figs. 5(c)
367 and 5(d)). During the resonant period, the changes in paral-
368 lel kinetic and gyro-kinetic energies due to the electromag-
369 netic wave are $\Delta T_{21} = \Delta E_{||\text{emw}} \approx -96.2 \times 10^{-5}$ eV, $\Delta U_{21} =$
370 $\Delta E_{\perp} \approx 39.3 \times 10^{-5}$ eV. The resulting energy transfer ratio
371 is given by $\frac{\Delta U_{21}}{\Delta T_{21}} \approx -0.408$. According to quantum theory, this ratio
372 is given by $\frac{\Delta U_{21}}{\Delta T_{21}} = -\frac{\hbar\omega_{ce}}{\hbar k \cdot v} \approx -0.3908$, where $\omega_{ce} \approx 3.51 \times$
373 10^9 s^{-1} , $k = 10^5 \text{ m}^{-1}$, and $v_z = 90 \text{ km/s}$. The quantum the-
374 ory prediction is in good agreement with the numerical results.
375 The derivation of this energy change ratio based on classical
376 theory is provided in the Appendix.

3.3. Validation of the relationship with wave angular momentum

378 Figures 6(a) and 6(b) show the velocity evolution under
379 linear polarization E_l , right-circular polarization E_R ($m = -1$),
380 and left-circular polarization E_L ($m = 1$). The work done on
381 the electron by the electromagnetic wave, E_{emw} , depicted in
382 Fig. 6(c), comprises the component along the parallel direc-
383 tion, $E_{||\text{emw}}$, as previously described, and the work on gyro-
384 kinetic energy, $E_{\perp\text{emw}}$. The latter is calculated as $E_{\perp\text{emw}} =$
385 $\int \mathbf{F}_{\perp} \cdot \mathbf{v}_{\perp} dt$, where \mathbf{F}_{\perp} is determined from the electric and
386 magnetic field forces, and \mathbf{v}_{\perp} represents the cyclotron velocity.
387 All these quantities can be obtained directly from the numer-
388 ical results and integrated discretely. As shown in Fig. (6(c)),
389 during the NDE period the electromagnetic wave performs
390 positive work on the electron, an effect analogous to photon
391 absorption. In contrast, during the ADE period the electro-
392 magnetic wave performs negative work, indicating that the
393 electron emits photons in a manner similar to stimulated emis-
394 sion.
395

396 The three polarization types are investigated under the
397 same scenario as before. As a result, the right-hand circularly
398 polarized (RHCP) wave ($m = 1$) induces a velocity change
399 only around $23\tau_{ce}$, whereas the left-hand circularly polarized
400

401 (LHCP) wave ($m = -1$) induces a velocity change only around
402 $113\tau_{ce}$. This confirms that the RHCP wave corresponds to the
403 NDE, while the LHCP wave corresponds to the ADE, in agree-
404 ment with the quantum analysis.

405 For a LHCP electromagnetic wave, the angular momen-
406 tum selection rule ($m = -1$) restricts resonance to occur only
407 when $\omega = \mathbf{k} \cdot \mathbf{v} - \omega_{ce}$, as confirmed numerically in Fig. 7. This
408 represents a significant departure from previous classical treat-
409 ments (Eqs. (36) and (37)),^[41] which allowed resonance at ar-
410 bitrary integer harmonics m , while remaining fully consistent
411 with quantum angular momentum conservation principles.

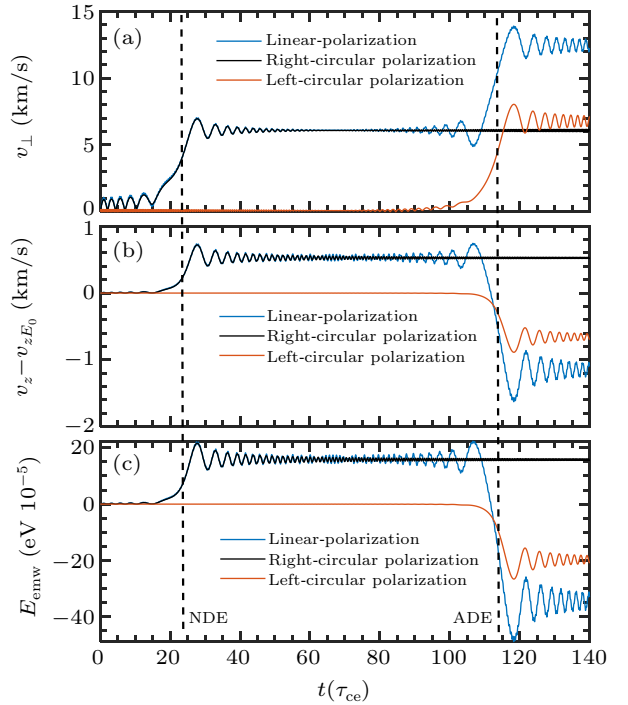


Fig. 6. Velocity evolution induced by waves with linear, right-circular, and left-circular polarization. (a) Cyclotron velocity v_{\perp} . (b) Change in parallel velocity caused by the electromagnetic wave. (c) Work done by the electromagnetic wave. NDE and ADE are marked by vertical dashed lines.

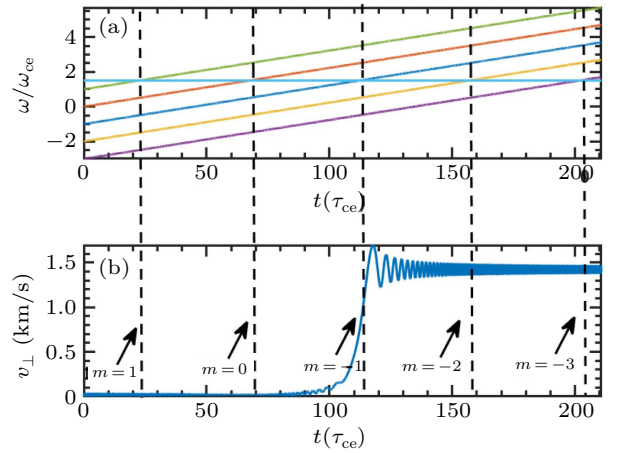


Fig. 7. (a) Frequency $\omega = \mathbf{k} \cdot \mathbf{v} + m\omega_{ce}$ for different m values and induced wave frequencies. (b) Evolution of perpendicular velocity under a left-circularly polarized wave ($m = -1$).

4. Discussion

Based on momentum and angular momentum conservation, let us consider the case where \mathbf{k} is oriented opposite to v_{\parallel} (or \mathbf{B}_0). In this scenario, if a cyclotron electron emits a photon with left-hand circular polarization and momentum $-\hbar\mathbf{k}$, carrying angular momentum \hbar , then after emission the change in internal energy is $\Delta U = -\hbar\omega_{ce} < 0$, while the change in translational kinetic energy is $\Delta T = \hbar kv_{\parallel} > 0$. In contrast, if the emitted photon has right-hand circular polarization with momentum $-\hbar\mathbf{k}$, the change in internal energy becomes $\Delta U = \hbar\omega_{ce} > 0$, while the translational kinetic energy remains $\Delta T = \hbar kv_{\parallel} > 0$. This scenario would violate energy conservation, since an electron cannot emit a photon while simultaneously increasing its total energy. Consequently, for a plane electromagnetic wave, only the left-circularly polarized component can resonate with an electron moving opposite to v_{\parallel} (or \mathbf{B}_0).

The resonant condition can also be interpreted classically. In the case of ADR, where $\mathbf{k} \parallel \mathbf{v}$ and $v_z > c' \equiv \omega/|\mathbf{k}|$, the LHCP wave appears as a right-hand polarized wave in the cyclotron electron's rest frame, allowing resonance. In contrast, for Normal Doppler Resonance, where $v_z < c'$, the RHCP wave maintains its polarization in the electron's rest frame. However, when \mathbf{k} is anti-parallel to \mathbf{v} ($\mathbf{k} \cdot \mathbf{v} < 0$), only the LHCP wave preserves the same rotational direction as the electron's cyclotron motion, independent of the parallel velocity. Therefore, in this configuration, only left-hand polarized waves can resonate with the electron.

This study also provides a perspective on electron heating and current drive by EM waves. During the NDR process, the fraction of the electron's internal energy gain from the EM wave relative to the total absorbed wave energy can be expressed as $\eta_H = \frac{m\omega_{ce}}{\omega}$, while the fraction contributing to parallel kinetic energy is $\eta_T = \frac{\mathbf{k} \cdot \mathbf{v}}{\omega}$. These relations can help optimize plasma heating and current drive efficiency. In the case of ADR, the electron's parallel kinetic energy can be converted into internal (gyro) energy, a mechanism that may contribute to suppressing runaway electron energies. This phenomenon has been studied previously,^[11,22] but further investigation is warranted in future fusion tokamak plasmas.

5. Conclusion

This paper presents a simple yet effective approach for analyzing resonant processes associated with the NDE and ADE. By combining quantum theory with angular momentum conservation analysis, it is demonstrated that the parameter m in the resonance condition $\omega = \mathbf{k} \cdot \mathbf{v} + m\omega_{ce}$ directly corresponds to the angular momentum of the resonant wave. Numerical simulations based on the Volume-Preserving Algorithm (VPA) further support the quantum results, confirming

both the angular momentum interpretation of m and the energy transfer characteristics. Future work will investigate the interaction between electron energy transformation and helicon waves in a plasma environment, aiming to provide deeper insights into applications such as plasma heating^[40] and suppression of runaway electrons.

Appendix A: Classical analysis of anomalous Doppler resonance

Neglecting the static electric field and relativistic effects, we provide a brief derivation of the energy transformation process based on classical dynamical equations

$$m_e \frac{d\mathbf{v}_{\parallel}}{dt} = -e(\mathbf{v}_{\perp} \times \mathbf{B}_{\perp}), \quad (\text{A1})$$

$$m_e \frac{d\mathbf{v}_{\perp}}{dt} = -e(\mathbf{v}_{\perp} \times \mathbf{B}_0 + \mathbf{v}_{\parallel} \times \mathbf{B}_{\perp} + \mathbf{v}_{\perp} \times \mathbf{B}_0). \quad (\text{A2})$$

Consider $\mathbf{B}_{\perp} = \frac{e_k \times \mathbf{E}_{\perp}}{v_p}$, where e_k is the unit vector along the wave vector of the electromagnetic wave, which is along the z -axis. Taking the dot product of \mathbf{v}_{\parallel} and \mathbf{v}_{\perp} with Eqs. (A1) and (A2), and substituting \mathbf{B}_{\perp} , we obtain

$$m_e \mathbf{v}_{\parallel} \cdot \frac{d\mathbf{v}_{\parallel}}{dt} = -e(\mathbf{v}_{\perp} \cdot \mathbf{E}_{\perp}) \frac{v_{\parallel}}{v_p}, \quad (\text{A3})$$

$$m_e \mathbf{v}_{\perp} \cdot \frac{d\mathbf{v}_{\perp}}{dt} = e(\mathbf{v}_{\perp} \cdot \mathbf{E}_{\perp}) \frac{v_{\parallel}}{v_p} - e(\mathbf{v}_{\perp} \cdot \mathbf{E}_{\perp}). \quad (\text{A4})$$

Here, $v_p = \omega/k$ is the phase velocity of the wave. Adding Eqs. (A3) and (A4) gives the total energy change of the electron

$$\frac{d}{dt} \left(\frac{1}{2} m_e v_{\parallel}^2 + \frac{1}{2} m_e v_{\perp}^2 \right) = -e(\mathbf{v}_{\perp} \cdot \mathbf{E}_{\perp}). \quad (\text{A5})$$

The sign of $-e(\mathbf{v}_{\perp} \cdot \mathbf{E}_{\perp})$ determines whether the electromagnetic (E.M.) wave undergoes "emission" ($-e(\mathbf{v}_{\perp} \cdot \mathbf{E}_{\perp}) < 0$) or "absorption" ($-e(\mathbf{v}_{\perp} \cdot \mathbf{E}_{\perp}) > 0$), depending on the phase difference between \mathbf{v}_{\perp} and \mathbf{E}_{\perp} .

From Eq. (A4) we have

$$e(\mathbf{v}_{\perp} \cdot \mathbf{E}_{\perp}) = \frac{m_e \mathbf{v}_{\perp} \cdot \frac{d\mathbf{v}_{\perp}}{dt}}{\frac{v_{\parallel}}{v_p} - 1}. \quad (\text{A6})$$

Substituting Eq. (A6) into Eq. (A3), we obtain

$$m_e \mathbf{v}_{\parallel} \cdot \frac{d\mathbf{v}_{\parallel}}{dt} = -\frac{m_e \mathbf{v}_{\perp} \cdot \frac{d\mathbf{v}_{\perp}}{dt}}{\frac{v_{\parallel}}{v_p} - 1} \frac{v_{\parallel}}{v_p}. \quad (\text{A7})$$

Integrating Eq. (A7), we obtain the classical invariant of motion for the electron under ADR

$$\frac{1}{2} m_e \left(v_{\parallel} - \frac{\omega}{k} \right)^2 + \frac{1}{2} m_e v_{\perp}^2 = C_0, \quad (\text{A8})$$

where C_0 is a constant determined by the initial conditions.

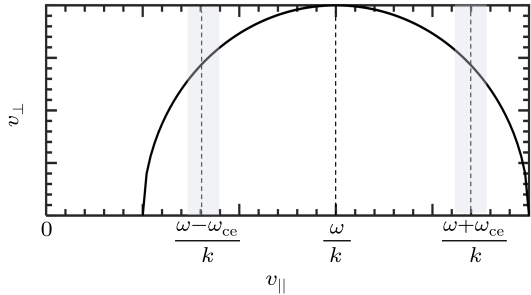


Fig. A1. Trajectory in the $(v_{\parallel}, v_{\perp})$ plane.

Here, C_0 refers to the initial value. The change in velocity is constrained to a circular trajectory, as illustrated in Fig. A1. At the NDR, where

$$v_{\parallel} = \frac{\omega - \omega_{ce}}{k},$$

an increase in v_{\parallel} corresponds to an increase in v_{\perp} . In contrast, at the ADR, where

$$v_{\parallel} = \frac{\omega + \omega_{ce}}{k},$$

an increase in v_{\parallel} corresponds to a decrease in v_{\perp} .

The change of energy in translational energy and gyro-kinetic energy can be written as

$$\frac{\Delta U}{\Delta T} = \frac{v_{\perp} dv_{\perp}}{v_{\parallel} dv_{\parallel}}. \quad (\text{A9})$$

From Eq. (A8), we have

$$\frac{dv_{\perp}}{dv_{\parallel}} = -\frac{v_{\parallel} - \frac{\omega}{k}}{v_{\perp}}. \quad (\text{A10})$$

Combining Eqs. (A9) and (A10), we obtain

$$\frac{\Delta U}{\Delta T} = -\frac{v_{\parallel} - \frac{\omega}{k}}{v_{\parallel}}. \quad (\text{A11})$$

According to the resonant condition

$$\omega = k v_{\parallel} + m \omega_{ce},$$

substituting v_{\parallel} into Eq. (A11) yields

$$\frac{\Delta U}{\Delta T} = \frac{m \omega_{ce}}{kv_{\parallel}}, \quad (\text{A12})$$

which agrees with the quantum result in Eq. (12).

Acknowledgment

This project is supported by the National Magnetic Confinement Fusion Energy Program of China (Grant No. 2019YFE03020001).

References

- [1] Tamm I E 1959 *Nobel Lectures* **18** 122
- [2] Frank I M 1960 *Science* **131** 702
- [3] Kiang D and Young K 2008 *Am. J. Phys.* **76** 1012
- [4] Ginzburg V L 1960 *Sov. Phys. Usp.* **2** 874
- [5] Shustin E G, Popovich P and Kharchenko I F 1971 *Sov. Phys. JETP* **59** 657
- [6] Nezlin M V 1976 *Sov. Phys. Usp.* **19** 946
- [7] Santini F, Barbato E and De Marco F 1984 *Phys. Rev. Lett.* **52** 1300
- [8] Kho T H and Lin A T 1988 *Phys. Rev. A* **38** 2883
- [9] Liu J, Wang Y and Qin H 2016 *Nucl. Fusion* **56** 064002
- [10] Wang Y, Qin H and Liu J 2016 *Phys. Plasmas* **23** 062505
- [11] Guo Z, McDevitt C J and Tang X Z 2018 *Phys. Plasmas* **25** 032504
- [12] Liu C, Hirvijoki E and Fu G Y 2018 *Phys. Rev. Lett.* **120** 265001
- [13] Shi X, Lin X and Kaminer I 2018 *Nat. Phys.* **14** 1001
- [14] Filatov L V and Melnikov V F 2021 *Geomagn. Aeron.* **61** 1183
- [15] Artsimovich L A, Bobrovskii G A and Mirnov S V 1967 *Sov. At. Energy* **22** 325
- [16] Kadomtsev B B and Pogutse O P 1968 *Sov. Phys. JETP* **26** 1146
- [17] Spong D A, Heidbrink W W and Paz-Soldan C 2018 *Phys. Rev. Lett.* **120** 155002
- [18] Liu Y, Zhou T and Hu Y 2019 *Nucl. Fusion* **59** 106024
- [19] Gorozhanin D V, Ivanov B I and Khoruzhiy V M 1997 *Waves excitation at anomalous Doppler effect for various electron beam energies*, Dec 31, 1997, Japan, pp. 402
- [20] Sajjad S 2007 *Chin. Phys. Lett.* **24** 3195
- [21] Castejon F and Eguilior S 2003 *Particle Dynamics under Quasi-linear Interaction with Electromagnetic Waves* (Madrid: Centro de Investigaciones Energeticas) p. 4
- [22] Zhang Q, Zhang Y, Tang Q and Tang X Z 2024 arXiv:2409.15830 [physics.plasm-ph]
- [23] Ginzburg N S 1979 *Radiophys. Quantum Electron.* **22** 323
- [24] Ginzburg V L 1996 *Phys. Usp.* **39** 973
- [25] Ginzburg V L 2005 *Acoust. Phys.* **51** 11
- [26] Coppi B, Pegoraro F, Pozzoli R and Rewoldt G 1976 *Nucl. Fusion* **16** 309
- [27] Frolov V P and Ginzburg V L 1986 *Phys. Lett. A* **116** 423
- [28] Arnaut H H and Barbosa G A 2000 *Phys. Rev. Lett.* **85** 286
- [29] Liu H, He X T, Chen S G and Zhang W Y 2004 arXiv:physics/0411183 [physics.plasm-ph]
- [30] Qian B L 1999 *IEEE Trans. Plasma Sci.* **27** 1578
- [31] Weyssow B 1990 *J. Plasma Phys.* **43** 119
- [32] Gogoberidze G and Machabeli G Z 2005 *Mon. Not. R. Astron. Soc.* **364** 1363
- [33] Roberts C S and Buchsbaum S J 1964 *Phys. Rev.* **135** A381
- [34] Bourdier A and Gond S 2000 *Phys. Rev. E* **62** 4189
- [35] Nusinovich G S, Korol M and Jerby E 1999 *Phys. Rev. E* **59** 2311
- [36] Nusinovich G S, Latham P E and Dumbrabs O 1995 *Phys. Rev. E* **52** 998
- [37] Qian B L 2000 *Phys. Plasmas* **7** 537
- [38] Zhang R, Liu J, Qin H, Wang Y, He Y and Sun Y 2015 *Phys. Plasmas* **22** 044501
- [39] Sha W E I, Lan Z, Chen M L N, Chen Y P and Sun S 2024 *IEEE J. Multiscale Multiphys. Comput. Tech.* **9** 113
- [40] Zhao Y, Bai J, Cao Y, Wu S, Ahedo E, Merino M and Tian B 2022 *Chin. Phys. B* **31** 075203
- [41] Dendy R O 1987 *Phys. Fluids* **30** 2438